NANO LETTERS

Letter

pubs.acs.org/NanoLett

Gate-Tunable Giant Stark Effect in Few-Layer Black Phosphorus

Yanpeng Liu,[†,‡] Zhizhan Qiu,[†,§] Alexandra Carvalho,[‡,∥] Yang Bao,[†,‡] Hai Xu,[†,‡] Sherman J. R. Tan,[†,§] Wei Liu,[†,‡] A. H. Castro Neto,[‡,∥] Kian Ping Loh,*[,†,‡] and Jiong Lu*[,†,‡]

[†]Department of Chemistry, National University of Singapore, 3 Science Drive 3, Singapore 117543

[‡]Centre for Advanced 2D Materials and Graphene Research Centre, National University of Singapore, Singapore 117546

[§]NUS Graduate School for Integrative Sciences and Engineering, National University of Singapore, 28 Medical Drive, Singapore 117456

[∥]Department of Physics, National University of Singapore, 3 Science Drive 2, Singapore 117542

S *Supporting Information*

ABSTRACT: Two-dimensional black phosphorus (BP) has sparked enormous research interest due to its high carrier mobility, layer-dependent direct bandgap and outstanding in-plane anisotropic properties. BP is one of the few two-dimensional materials where it is possible to tune the bandgap over a wide energy range from the visible up to the infrared. In this article, we report the observation of a giant Stark effect in electrostatically gated few-layer BP. Using low-temperature scanning tunnelling microscopy, we observed that in few-layer BP, when electrons are injected, a monotonic reduction of the bandgap occurs. The injected electrons compensate the existing defect-induced holes and achieve up to 35.5% bandgap modulation in the light-doping regime. When probed by tunnelling spectroscopy, the local density of states in few-layer BP shows characteristic resonance features arising from layer-dependent sub-band structures due to quantum confinement effects. The demonstration of an electrical gate-controlled giant Stark effect in BP paves the way to designing electro-optic modulators and photodetector devices that can be operated in a wide electromagnetic spectral range.

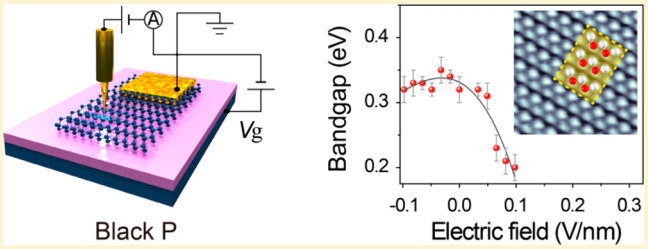

KEYWORDS: *Black phosphorus, giant Stark effect, bandgap, electrostatical-gating, scanning tunnelling microscopy*

The Stark effect is the shifting and splitting of atomic energy levels under the influence of an externally applied electric field. In semiconductors, in the presence of an electric field the Stark effect will cause the energy levels to shift, which in turn modifies the bandgap. Hence, by changing the electric field, the electro-optical response of the material can be tuned.[1,2] In quantum-confined systems, the Stark effect often gives a strong optical bandgap modulation due to inhibited exciton field ionization and reduced field screening as opposed to that in bulk materials.[3,4] The quantum-confined Stark effect (QCSE) is the basis on which III−V semiconductor-based optical modulators operate.[3] However, the relatively low energy offset between the quantized transitions and the surrounding cladding (such as GaAs with a bandgap ∼1.52 eV at 4 K) means that even operational fields greater than only a few tens of kV cm^{-1} can cause the tunnelling-out of the electrons to occur.[4] Some two-dimensional (2D) materials can potentially show a stronger Stark effect beyond those encountered in quantum-well structures due to its weaker dielectric screening, and its strongly anisotropic properties. However, it is difficult to induce a semiconductor-to-metal transition in bilayer transition metal dichalcogenides (TMDs) by tuning the externally applied electric field because of the relatively large bandgap (≥1 eV) of these materials with the critical external electric field for such a transition being in the range 2−3 V/nm.[5]

Black phosphorus (BP), a layered allotropic form of elemental phosphorus, has attracted increased attention from researchers because of its layer-dependent bandgap spanning the entire electromagnetic spectrum, which is unmatched by any other 2D material known to date.[6−12] BP has both high mobility and a thickness-dependent direct bandgap (∼2.0 eV for monolayer and ∼0.3 eV for bulk sample owing to the strong interlayer coupling).[12−14] In view of its orthorhombic crystal lattice with a puckered honeycomb structure, the conduction band minimum (CBM) and the valence band maximum (VBM) of BP are mainly contributed by localized P $3p_z$ orbitals (vertical to the puckered plane) rather than by $3p_x$ and $3p_y$, which means that the electronic properties of BP are very sensitive to electric field applied perpendicularly.[15] The Stark effect coefficient is a parameter that reflects the rate of the reduction of band gap with applied field strength. The small bandgap (∼0.3 eV in multilayer or bulk limit) and monotonically increasing Stark effect coefficient with layer number allows the semiconductor-to-metal transition of few-layer BP to be achieved at a relatively low critical field, for instance, the critical

Received: December 28, 2016
Revised: February 13, 2017
Published: February 14, 2017

DOI: 10.1021/acs.nanolett.6b05381
Nano Lett. 2017, 17, 1970−1977

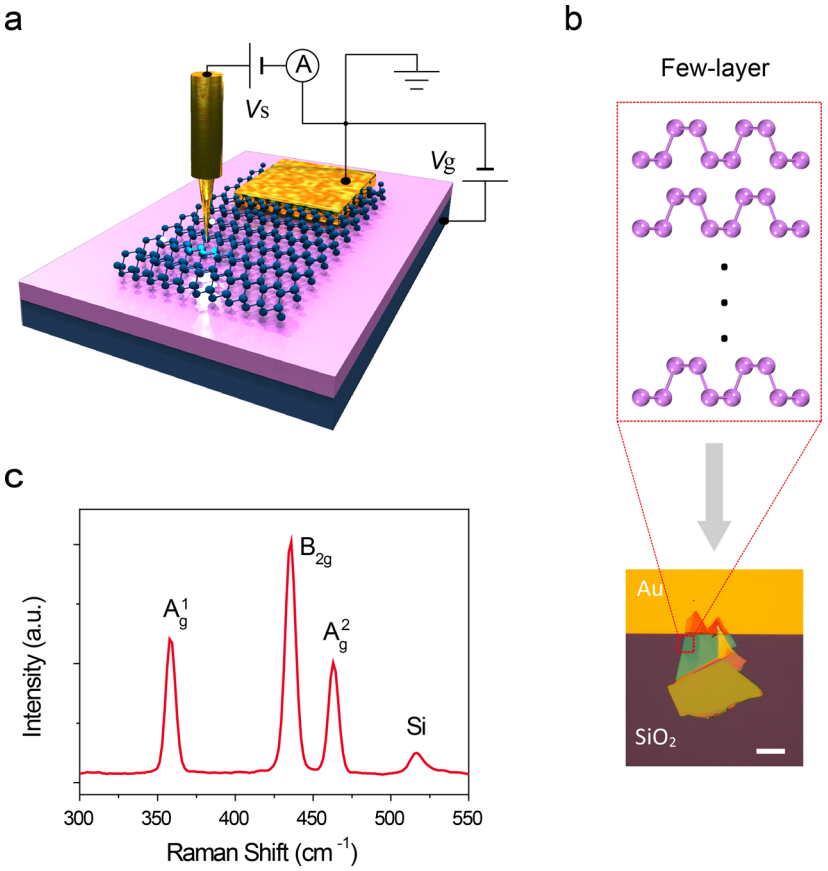

Figure 1. Schematic drawing and structural characterization of a few-layer BP device. (a) Schematic illustration of a gated BP device during STM analysis. The sample bias V_S is applied between the STM tip and the thin BP sample contacted by a gold electrode. The electrostatic gate voltage is applied to the BP flake through a p-doped silicon wafer. (b) Optical image of few-layer BP flakes on silicon substrate partially in contact with a gold electrode. Scale bar is 20 μm. (c) Raman spectrum of the as-prepared BP flake; the peak at ~520 cm^{-1} originates from the underlying silicon substrate.

field $E_c \approx 0.68$ V/nm for 10 layers.[15,16] In addition, according to nonlinear Thomas-Fermi theory, in view of the moderate screening effects of BP, the BP flakes thinner than 10 nm will be strongly perturbed by an applied external electrical field.[17] Recently, potassium dopant has been used to tune the electronic bandgap of bulk BP and the transition from a moderate-gap semiconductor to a band-inverted semimetal was induced by applying an ionization-induced vertical electric field.[18] It has also been demonstrated that introducing surface transfer dopants such as cesium carbonate and molybdenum trioxide or depositing cross-linked poly(methyl methacrylate) on BP surface is capable of tuning the transport properties of BP.[19,20] However, the drawbacks of chemical doping include instability in air and increased probability of introducing charged scattering centers. In addition, it is difficult to achieve reversible doping using chemical dopants. In contrast, electrostatic doping, which is continuously tunable, nondestructive, and carried out in ambient atmosphere, has been widely adopted to tune the optoelectronic properties of 2D materials and their heterostructures.[21−30] It has been predicted from theory that the electrical and optical properties of ultrathin BP can be effectively tuned by electrostatic doping.[15,16,31,32] However, difficulties in the preparation of 2D BP device and its high reactivity when exposed to air have so far limited systematic experimental investigations.[28−30,33−36]

Here, we report a low-temperature scanning tunneling microscopy (LT-STM) study on a few-layer BP device to demonstrate a giant Stark effect in few-layer BP flakes induced by electrostatic gating. We find that the application of an external perpendicular electric field across few-layer BP flakes leads to a monotonic narrowing of the bandgap with increasing field intensity. We achieve a notable bandgap reduction of ~35.5% (from 310 ± 20 to 200 ± 20 meV) by applying a vertical field of 0.1 V/nm. It is expected therefore that few-layer BP can be transformed from moderate-gap semiconductor to a band-inverted semimetal under a more intense electric field. Furthermore, we observe resonance features in the dI/dV spectra, which originate from the thickness-dependent subband structures in few-layer BP. The gate tunable Stark effect of BP implies that it can be used as an electro-optical modulator operating in the far and mid-infrared regions.

To probe the effect of the applied electric field on the electronic properties of BP, we prepared a field effect transistor (FET) device consisting of a few-layer BP flake stacked on a SiO_2 substrate with a doped Si back gate as shown in Figure 1a (see methods in Supporting Information for more details). Using the well-established dry transfer technique, a few-layer BP flake was placed on the surface of a prepatterned gold electrode deposited on a SiO_2/Si substrate.[37] The gold electrode served as the electrical contact required for STM measurements (Figure 1b). The crystallinity of the BP flake was characterized using Raman spectroscopy. Figure 1c shows the Raman spectrum with the three intrinsic peaks at ~362.9, 438.7, and 467.4 cm^{-1}, which are attributed to the A_g^1, B_{2g}, and

DOI: 10.1021/acs.nanolett.6b05381
Nano Lett. 2017, 17, 1970−1977

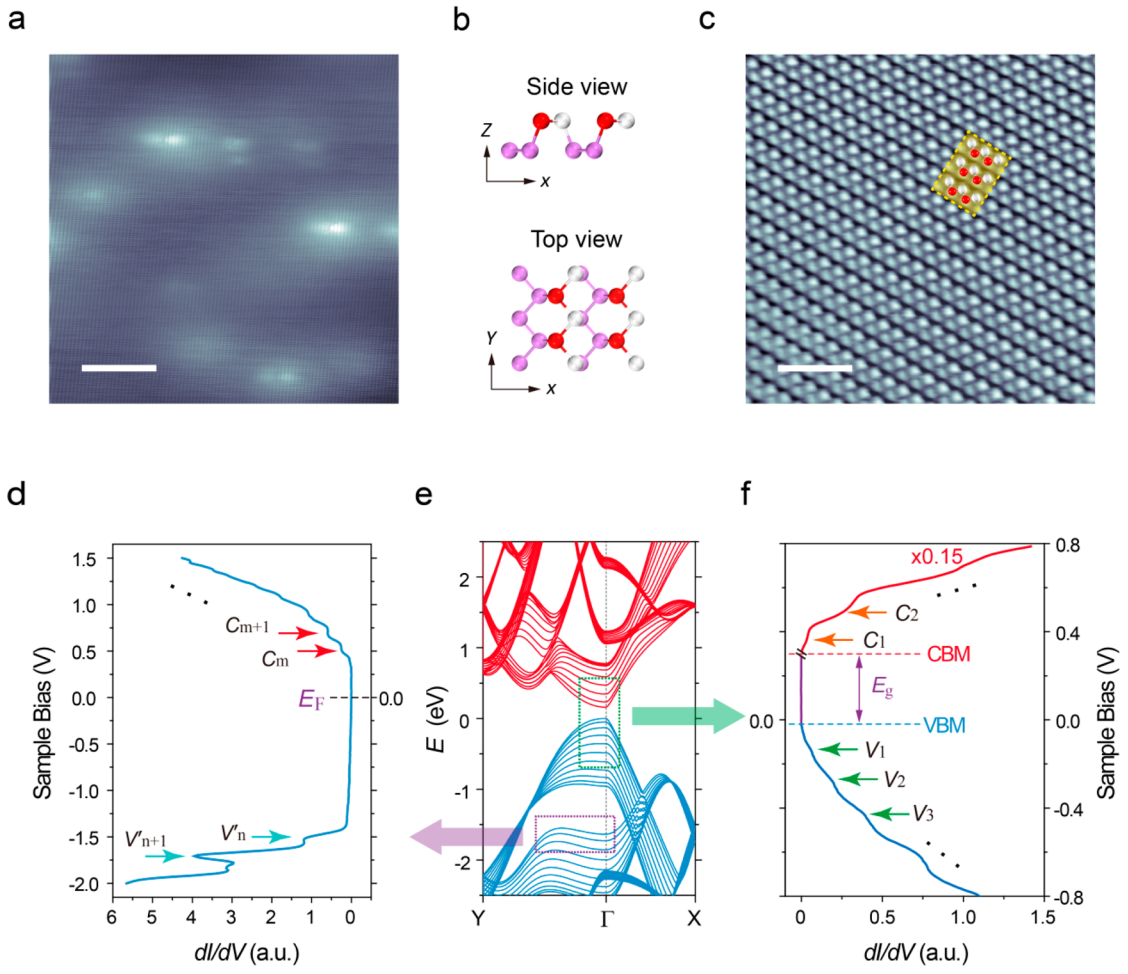

Figure 2. STM imaging and electronic characterization of a few-layer BP device. (a) Large-area STM imaging of the bare BP flake (V_S = −0.3 V, I = 0.6 nA). Scale bar is 10 nm. (b) Sketches showing the side and top view of monolayer BP. Scale bar is 10 nm. (c) High-resolution STM image of BP (V_S = −0.35 V, I = 0.8 nA). Scale bar is 1.5 nm. (d) A wide energy range dI/dV spectrum acquired on few-layer BP showing the electronic resonance features V'_n in the valence band and C_m in the conduction band. E_F represents Fermi energy (set point: V_S = −2.0 V, I = 2.5 nA). (e) PBE band structure calculation of 11-layer BP. (f) A narrow energy range dI/dV spectrum taken on the same spot (as that in d) revealing the valence band maximum, the conduction band minimum, and a few resonance peaks (V_n in VB region and C_m in CB region). CB region (red line) is rescaled by a factor of 0.15 for visual contrast.

A_g^2 phonon modes, respectively, in few-layer BP resulting from its orthorhombic crystal structure (shown in the upper panel of Figure 1b).[7,11,38] To minimize surface degradation, BP devices were immediately loaded into the LT-STM chamber after device fabrication. The thickness of BP flakes probed in our STM study was determined to be equivalent to 11 layers using atomic force microscopy (AFM) (see Supporting Information Figure S1).

Figure 2a shows a typical STM topographic image of a thin BP flake for a scan area of 50 nm × 50 nm. It is seen that arrays of one-dimensional (1D) zigzag atomic rows corresponding to the upper rows of atoms in the puckered BP layer are clearly resolved, similar to the atomic STM images of in situ cleaved bulk BP sample in previous reports.[39,40] Our high-resolution STM images reveal that an intact BP lattice is present in a majority of the flat surface regions. The defect-related feature showing a bright topographic contrast in STM imaging (Figure 2a) is presumably due to buried impurities or atomic substituents in the BP host lattice. These defects may contribute to hole doping in pristine BP crystals; this aspect is described in a later section.

According to the atomic structural model of BP (Figure 2b), each P atom is covalently bonded to three nearest neighbor atoms through 3p orbitals to form a puckered structure consisting of an upper row of P atoms (red and white balls) and a lower row of P atoms (violet balls).The wave function of the lower P atoms is expected to decay exponentially in the vertical direction and thus only the P atoms located on the top are clearly resolved in the STM topographic image as shown in the close up image (Figure 2c). The lattice constants measured along two directions (armchair "xx" and zigzag "xy" shown in Figure 2b, top view) are determined to be 4.46 ± 0.13 and 3.32 ± 0.05 Å, respectively, which are in good agreement with previously reported values for bulk BP.[12,13,39,40] Figure 2d shows a wide energy range dI/dV spectrum (which reflects the local density of states, LDOS) collected from areas on the BP surface far away from defective regions. The intrinsic spectrum is highly asymmetric and shows a wide "gaplike" signature surrounded by a series of well-defined resonant peaks labeled as V_n in the valence band and C_m in the conduction band. The origin of these prominent resonance features will be discussed later in the article. Because of the relatively large tip−sample separation, the dI/dV signal in the vicinity of the Fermi energy

DOI: 10.1021/acs.nanolett.6b05381
Nano Lett. 2017, 17, 1970−1977

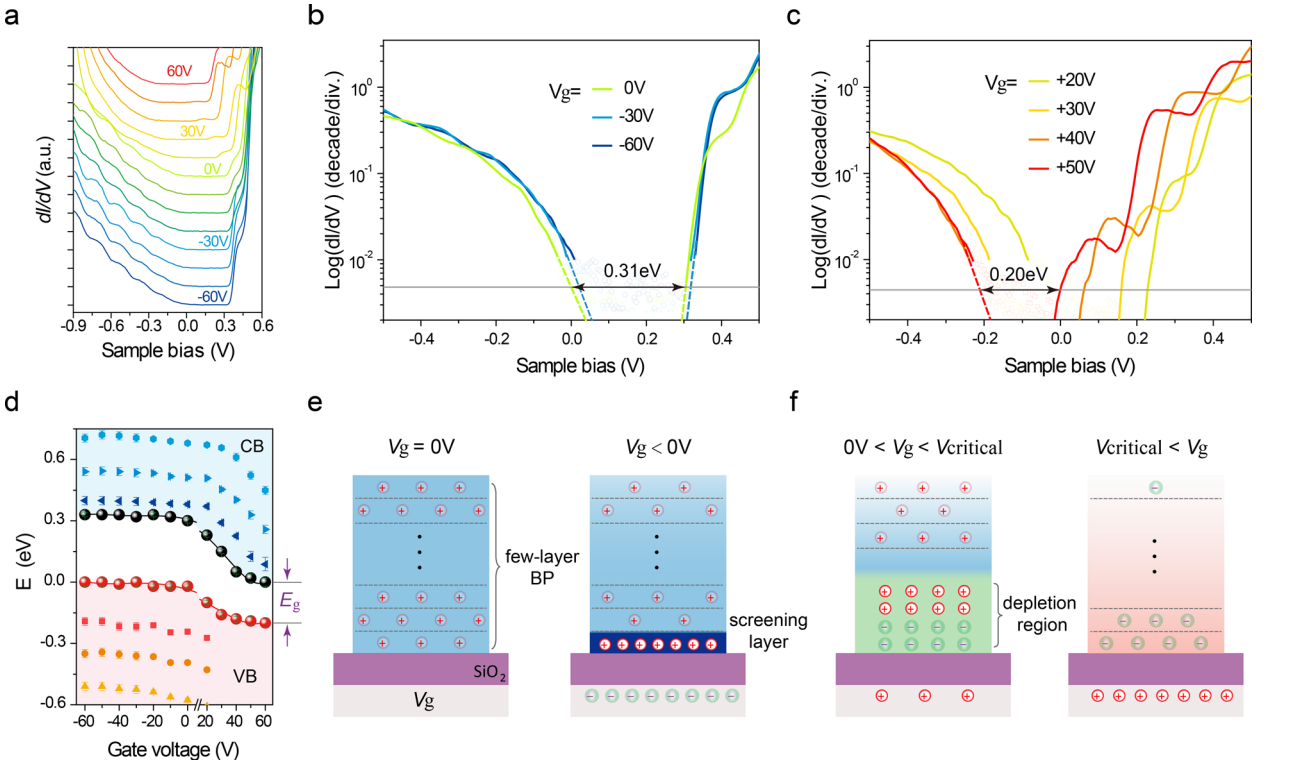

Figure 3. Gate-controlled Stark effect in an 11-layer BP flake device. (a) Gate-dependent dI/dV spectra obtained on a defect free region in an 11-layer BP flake. (Set point: V_S = −1.0 V, I = 1.0 nA). The curves are vertically offset and the gate voltage step is 10 V. (b,c) Logarithmic dI/dV spectra under negative and positive gate voltages, respectively. (d) VBM (red balls), CBM (black balls), resonance peaks (solid symbols), and bandgap (E_g) of 11-layer BP at different gate voltages. (e,f) Schematic models (note: thickness and charge carrier density not to scale) to illustrate the charge carrier distribution and gate-dependent behavior of 11-layer BP shown in panels b and c, respectively.

(E_F, V_S= 0 V) is low and thus the prominent features in the spectrum occurs at high energy away from E_F.[21,39−41] To better resolve the electronic states close to E_F, a lower set point (V_S = −1.0 V, I = 1.0 nA) has been used to collect the dI/dV spectrum from the same surface region as shown in Figure 2f. The bandgap of the as-prepared BP ($E_g = E_{CBM} - E_{VBM}$, see Supporting Information Figure S2 for details of the calculation) is determined to be 310 ± 20 meV, which is consistent with previously reported behavior and values for bulk BP.[12,40] The slight fluctuation of E_g may be attributed to a tip-induced band bending effect, which has been carefully investigated in this work (see Supporting Information for details). Our STS data also reveal that the as-prepared BP flakes are heavily p-doped, which is confirmed from the closeness of the VBM energy and E_F (Figure 2f).

Next, we probe the evolution of the local electronic properties of BP as a function of the applied back gate voltage (V_g). In contrast to n-doping using K atoms, electrostatic gating enables us to tune the doping levels in thin BP flakes to obtain p-type or n-type behavior.[18] Figure 3a shows the gate-voltage-dependent STS spectra acquired in the defect-free region of the 11-layer BP flake. At positive gate voltages (V_g > 0 V), negative charge carriers are injected into the BP flake leading to n-type doping of BP. Hence, the band structure shifts toward the negative sample bias region [from the green line (0 V) up to the red line (+60 V)]. To our surprise, the shift of the band structure toward higher potential energy [(from the green line (0 V) down to the blue line (−60 V)] is negligible. This observation is tentatively attributed to the heavily p-doped nature of the thin BP flakes (E_F is located at the edge of the VB and the presence of shallow acceptor states), which leads to Fermi level pinning. In order to determine the values of the VBM, CBM and bandgap more accurately, the logarithm of the dI/dV spectra collected at different gate voltages on thin BP flakes were plotted (shown in Figure 3b,c) (refer to Supporting Information Figure S2 for more details). Using this method, we extracted the gate-dependent energies corresponding to CBMs, VBMs, and the resonance peaks as shown in Figure 3d. It can be clearly observed that the CBMs and VBMs (pinned at the E_F) barely shift at $V_g \leq 0$ V and, consequently, the overall shift in the band structure of BP is negligible. In contrast, at $V_g \geq 0$ V, a pronounced downward shift of the entire band structure is observed. Interestingly, we also observed that the bandgap reduces significantly with increase in applied gate voltages at $V_g \geq 0$ V. In addition, the observed resonance peaks at different gate voltages move with the band edges depending on whether they are in the conduction band or the valence band region.

Here we employ scanning tunneling spectroscopy (STS) to measure field-dependent single-particle electronic bandgap of few-layer BP as opposed to two-particle optical bandgap via optical adsorption.[41] Hence, the reduction in the bandgap of 11-layer BP flakes as a function of gate voltages can be explained on the basis of a giant Stark effect rather than Franz-Keldysh effect reported in the recent work on optoelectronic modulation of BP.[28,29,42] In the absence of a giant Stark effect, a rigid band shift typically occurs with gate voltage and E_g remains unchanged even when electric field is applied (Figure 4a, left. $E_g = E'_g$ = constant).[24,43] In the presence of the Stark effect, the band edges of VB and CB gradually move toward each other with increasing gate voltage due to the spatial redistribution of their wave functions in the puckered layer structure, as shown in Figure 4a (right). To understand the

DOI: 10.1021/acs.nanolett.6b05381
Nano Lett. 2017, 17, 1970−1977

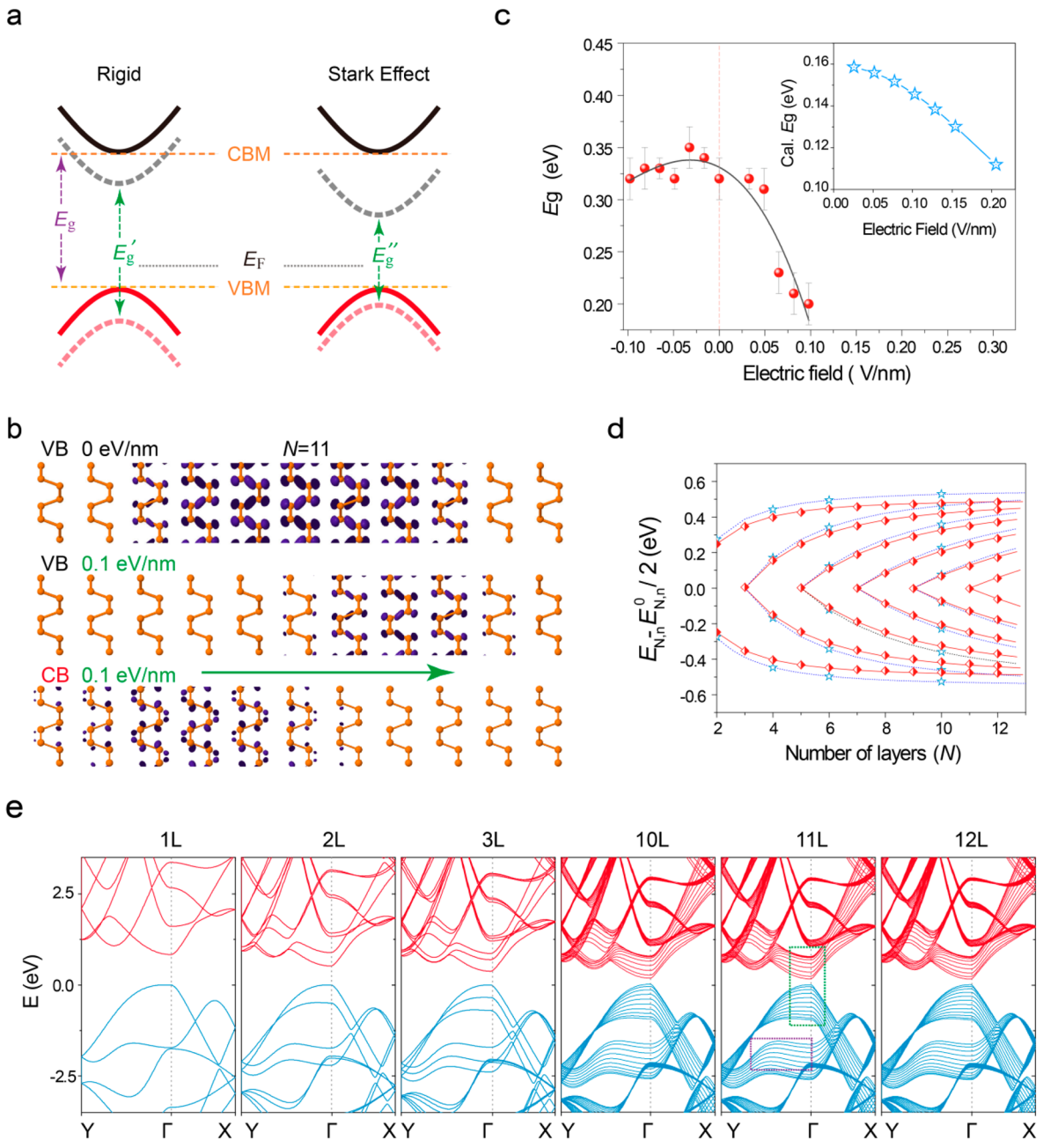

Figure 4. Calculated electronic structures of few-layer BP with and without field modulation. (a) Schematic illustration of the field modulation of electronic structures of few-layer BP with and without a giant Stark effect. The solid red and black lines indicate the initial positions of VBM and CBM (E = 0 V) while the dashed red and black lines represent the VBM and CBM under an electric field ($E \neq 0$ V), respectively. (b) The wave function modulus square of the highest occupied state at Γ point for 11-layer BP sample at 0 V/nm (top) and 0.1 V/nm (middle) electrical fields. The wave function modulus square of the lowest unoccupied state at Γ point for the 11-layer BP sample at 0.1 V/nm electrical field (bottom). (c) Measured bandgap of 11-layer BP as a function of applied electrical field. Inset shows the calculated bandgap of a BP sample of the same thickness in the presence of electrical fields of different strength. (d) Level spacing in few-layer BP (layer number N = 2−12) obtained from PBE (red) and HSE (blue) calculation methods. (e) Representative layer-dependent PBE band structures of BP; please refer to the Supporting Information Figure S7 for a more detailed version of the calculation.

asymmetry in gap reduction observed in Figure 3a,d, we provide a schematic to explain the experimental results at different gate bias. Initially (V_g = 0 V, left panel of Figure 3e), the few-layer BP sample is p-doped (VBM of BP flake nearly touches the Fermi energy, Figure 2f and green line in Figure 3b) and therefore, free positive charge carriers distribute uniformly in the real space of few-layer BP. When a negative gate voltage is applied (V_g < 0 V, electrons accumulate in the p ++ silicon layer and thus holes will be induced in the BP layers), additional holes fill the valence states. As a result of the accumulation of holes, screening of the gate electric field occurs (right panel in Figure 3e) and the measured bandgap of BP remains approximately constant (Figure 3b). On the other hand, a positive gate voltage injects electrons into the BP flake. A depletion layer is formed with different heights depending on the field strength (left panel, Figure 3f), which facilitates the penetration of the electric field into the whole BP flake (right panel, Figure 3e). During this process, two effects can occur: (i)

DOI: 10.1021/acs.nanolett.6b05381
Nano Lett. 2017, 17, 1970−1977

a potential drop that shifts the CB and the VB toward lower energy and (ii) a gap reduction due to the Stark effect as shown in Figure 3c (V_g = 0, 20, and 30 V). With increasing voltage (E_F locates right in the middle of bandgap, here, V = 29 ± 1 V), the holes become completely depleted by back-gating. At even higher positive gate voltages, the BP flake becomes electron doped, (as shown in Figure 3f, right panel) and both the VB and the CB move toward the negative sample bias region with the latter approaching the Fermi level. Once the CB touches the Fermi level, the "pinning" effect dominates and the gap reduction is arrested. For the latter two cases shown in Figure 3f (V_g > 0 V), the bandgap of few-layer BP is reduced to 200 ± 20 meV even at a moderate gate voltage (V_g = 60 V), due to the giant Stark effect.[1,2,16] The magnitude of bandgap modulation achievable by the Stark effect is predicted to be larger in thinner BP flakes due to its larger bandgap as compared to thicker BP, where electro-optical modulation from the visible to far-infrared regime can be achieved in monolayer and bilayer BP.[7,15,16] Our theoretical calculations reveal that the Stark coefficient defined as $S_{nL} = -(dE_g/dE_{ext})/e$ increases monotonically as a function of layer thickness (see Supporting Information Figure S3), suggesting that a large critical field strength is required to induce the semiconductor-to-semimetal phase transition for thinner samples.

In order to estimate the magnitude of reduction of E_g by Stark effect and to identify the origin of the resonance peaks in the dI/dV spectra, we calculate the electronic structure of few-layer BP under different external electrical fields, using density functional theory (DFT) calculations within the Perdew–Burke–Ernzerhof parametrization (PBE).[12,16] Figure 4b shows the highest occupied states at the Γ-point for an 11-layer BP sample without (top) and with (bottom) 0.1 V/nm electrical field, where a strong redistribution of the VBM states along the z-direction is observed in the latter. Even though the value of the estimated bandgap is slightly underestimated using the PBE approximation, modifications of the band structure due to small perturbations can be correctly predicted. For low fields, it is found that the bandgap varies quadratically with the electric field as expected from the system symmetry. Because phosphorene is centrosymmetric and has no dipole in the direction of the field, the first order term in the expression for the energy levels ε_i in E vanishes, and the leading terms (as found by perturbation theory) are given by

$$\varepsilon_i = \varepsilon_i^0 + \sum_{k \neq i} \frac{M_{ik}^{zz}}{\varepsilon_i - \varepsilon_k} E^2 \quad (1)$$

where M_{ik}^{zz} is the dipole matrix element between states i and k.

This is qualitatively similar to the experimentally observed behavior (Figure 4c). If the intensity of the electric field is calculated from the experimental values for V_g assuming that the system can be approximated by two planar capacitors in series (see Supporting Information Figure S4 for more details), the experimentally obtained rate dE_g/dE is of the same order of magnitude as expected from the theoretical prediction (inset in Figure 4c), despite the bandgap underestimation, the uncertainty in the estimation of the capacitance, and tip-induced band bending effects that may contribute to decrease the measured dE_g/dE.[24,44,45] In fact, a large magnitude of bandgap reduction should be achievable by applying a high electric field. By performing transport studies on a dual-gated BP transistor, Deng et al. reported that the band gap can be narrowed to ∼50 meV under a high electric field strength of 1.1 V/nm by measuring the minimum transport conductivity and carrier density at different temperatures.[30]

In the STS spectra (Figure 2d,f) of the 11-layer BP flake, in addition to the gap feature, resonance peaks are observed. The tendency of these peaks to move in the same direction as the band edges as a function of the gate voltage indicates that they originate from electronic states and are not due to tip-induced charging effects (see Supporting Information Figure S5).[22,41] The energy separation between the adjacent resonances observed here is larger than 150 meV, which is much higher than the energy of the most energetic phonon mode of BP (∼66.1 meV).[38] The nearly rigid shifting of the resonance peaks together with the band edges also rules out possible contribution from electron-plasmon coupling (see Supporting Information for more details on other possible origins of these peaks).[46−48] Instead, a sub-band model due to the quantisation of BP layers with finite thickness can be used to explain the thickness-dependent resonance features in the STS spectra, which is verified both by our DFT calculations with PBE and through a phenomenological tight-binding model.[14,49] LDOS obtained from DFT calculations are in good agreement with the STS spectra recorded on BP with different layer numbers (see Supporting Information Figure S6). Because of the strong interlayer interaction, both the CBs and VBs of N-layer phosphorene are quantized and split into N 2D sub-bands. This quantum-well-like structure creates the characteristic sub-band structures of few-layer BP, which in turn modifies its density of states. In the absence of other interactions and thermal effects, this density of states (DOS) modulation may manifest as singularities in a system with a parabolic band dispersion. The spacing between the peaks can be approximated by a simple one-dimensional tight-binding band model

$$E_{N,n} = E_{N,n}^0 + 2\gamma \cos\left(\frac{n\pi}{N+n}\right) \quad (2)$$

where n = 1, 2···, N, is the subband index, $E_{N,n}^0$ is the average band energy, and γ = 0.55 (HSE), 0.49 (PBE). On the basis of this simplified tight-binding model, an integrated evolution of the sub-band structures of few-layer BP is empirically described (Figure 4d). This model describes the band energy at the Γ point of the 2D Brillouin zone considering only the nearest-neighbor layer–layer interaction while neglecting electron–electron and electron–hole (exciton effect) interactions, in accordance with our experimental conditions.

To further elucidate the nature of the resonance peaks in STS, we compare the experimental dI/dV spectra with the DOS obtained from DFT calculations for few-layer BP ranging from 1–12 layers (Figure 4e, see Supporting Information Figure S7 for a full version). The large hole effective mass along the Γ–Y direction leads to additional contributions in DOS, which gives rise to the observed peaks in STS (shown in Figure 2f). Moreover, the sharp peaks that are seen appearing in the −1.5 to −2 eV energy range (V'_n, Figure 2d) originate from deep-lying flat sub-bands. Our calculations confirm the presence of sub-bands with energy spacing similar to the experimentally observed resonance peaks. One remarkable feature is the possibility for optical transitions between quantized sub-bands in the same band, leading to multiphoton absorptions. The unique sub-band structure also suggests that BP may qualify as an emerging candidate material for quantum cascade lasers.[50]

The giant Stark effect in few-layer BP device allows the bandgap of BP to be electrically tuned. For 11-layer-thick BP,

DOI: 10.1021/acs.nanolett.6b05381
Nano Lett. 2017, 17, 1970−1977

the bandgap can be reduced from 310 ± 20 to 200 ± 20 meV. Interestingly, layer-dependent sub-band structures (especially the sub-bands at Γ-point) have been experimentally observed in our STS measurements, where we found that the number of sub-bands is directly correlated to the number of layers in BP. This suggests that STS can be used as a tool to accurately determine the layer number in few-layer BP. The reduced bandgap of few-layer BP due to the giant Stark effect shifts its working spectral range to far-IR while the sub-band transition induces multiphoton absorptions.[50−52] Moreover, the giant Stark effect breaks the symmetric BP quantum well-like electronic structure, leading to the relaxation of selection rules and consequently activates "forbidden" optical transitions from the valence sub-band to the conduction sub-band with different quantum numbers.[52] Our work suggests that the interband and inter-sub-band transitions in BP can be continuously varied over a wide electromagnetic spectral range from visible to far IR by varying the electric field, making BP a versatile material platform for applications in IR optical modulators and quantum cascade lasers.

■ ASSOCIATED CONTENT

Supporting Information

The Supporting Information is available free of charge on the ACS Publications website at DOI: 10.1021/acs.nanolett.6b05381.

Details of the experiment method, thickness determination, bandgap calculation method, layer-dependent properties of BP, exclusion of possible origin of resonance peaks, calculated band structure of 1−12 layer BP (PDF)

■ AUTHOR INFORMATION

Corresponding Authors

*(K.P.L.) E-mail: chmlohkp@nus.edu.sg.
*(J.L.) E-mail: chmluj@nus.edu.sg.

ORCID

Yang Bao: 0000-0001-9868-4946
Kian Ping Loh: 0000-0002-1491-743X
Jiong Lu: 0000-0002-3690-8235

Author Contributions

Y.L., Z.Q., and A.C. contributed equally to this work.

Notes

The authors declare no competing financial interest.

■ ACKNOWLEDGMENTS

The authors acknowledge the National Research Foundation, Prime Minister Office, Singapore, under its Medium Sized Centre Programme and CRP award "Novel 2D materials with tailored properties: Beyond graphene" (R-144-000-295-281). The first-principles calculations were carried out on the Centre for Advanced 2D Materials computing facilities. J. Lu acknowledges the support from NUS start-up grant (R-143-000-621-133) and Tier 1 (R-143-000-637-112).

■ REFERENCES

(1) Park, C.-H.; Louie, S. G. *Nano Lett.* **2008**, *8*, 2200−2203.
(2) Khoo, K. H.; Louie, S. G. *Phys. Rev. B: Condens. Matter Mater. Phys.* **2004**, *69*, 201401.
(3) Kuo, Y.; Lee, Y. K.; Ge, Y.; Ren, S.; Roth, J. E.; Kamins, T. I.; Miller, D. A. B.; Harris, J. S. *Nature* **2005**, *437*, 1334−1336.
(4) Fröhlich, D.; Wille, R.; Schlapp, W.; Weimann, G. *Phys. Rev. Lett.* **1987**, *59*, 1748.
(5) Ramasubramaniam, A.; Naveh, D.; Towe, E. *Phys. Rev. B: Condens. Matter Mater. Phys.* **2011**, *84*, 205325.
(6) Li, L.; Yu, Y.; Ye, G. J.; Ge, Q.; Ou, X.; Wu, H.; Feng, D.; Chen, X. H.; Zhang, Y. *Nat. Nanotechnol.* **2014**, *9*, 372−377.
(7) Ling, X.; Wang, H.; Huang, S.; Xia, F.; Dresselhaus, M. S. *Proc. Natl. Acad. Sci. U. S. A.* **2015**, *112*, 4523−4530.
(8) Churchill, H. O.; Jarillo-Herrero, P. *Nat. Nanotechnol.* **2014**, *9*, 330−331.
(9) Liu, H.; Du, Y.; Deng, Y.; Peide, D. Y. *Chem. Soc. Rev.* **2015**, *44*, 2732−2743.
(10) Reich, E. S. *Nature* **2014**, *506*, 19.
(11) Castellanos-Gomez, A. *J. Phys. Chem. Lett.* **2015**, *6*, 4280−4291.
(12) Qiao, J.; Kong, X.; Hu, Z. X.; Yang, F.; Ji, W. *Nat. Commun.* **2014**, *5*, 4475.
(13) Low, T.; Rodin, A. S.; Carvalho, A.; Jiang, Y.; Wang, H.; Xia, F.; Neto, A. C. *Phys. Rev. B: Condens. Matter Mater. Phys.* **2014**, *90*, 075434.
(14) Li, L.; Kim, J.; Jin, C.; Ye, G.; Qiu, D. Y.; da Jornada, F. H.; Shi, Z.; Chen, L.; Zhang, Z.; Yang, F.; Watanabe, K. *Nat. Nanotechnol.* **2016**, *12*, 21−25.
(15) Li, Y.; Yang, S.; Li, J. *J. Phys. Chem. C* **2014**, *118*, 23970−23976.
(16) Dolui, K.; Quek, S. Y. *Sci. Rep.* **2015**, *5*, 11699.
(17) Low, T.; Roldán, R.; Wang, H.; Xia, F.; Avouris, P.; Moreno, L. M.; Guinea, F. *Phys. Rev. Lett.* **2014**, *113*, 106802.
(18) Kim, J.; Baik, S. S.; Ryu, S. H.; Sohn, Y.; Park, S.; Park, B. G.; Denlinger, J.; Yi, Y.; Choi, H. J.; Kim, K. S. *Science* **2015**, *349*, 723−726.
(19) Wang, G.; Bao, L.; Pei, T.; Ma, R.; Zhang, Y. Y.; Sun, L.; Zhang, G.; Yang, H.; Li, J.; Gu, C.; Du, S. *Nano Lett.* **2016**, *16*, 6870.
(20) Xiang, D.; Han, C.; Wu, J.; Zhong, S.; Liu, Y.; Lin, J.; Zhang, X.-A.; Ping, H. W.; Özyilmaz, B.; Neto, A. H. C. *Nat. Commun.* **2015**, *6*, 6485.
(21) Zhang, Y.; Brar, V. W.; Wang, F.; Girit, C.; Yayon, Y.; Panlasigui, M.; Zettl, A.; Crommie, M. F. *Nat. Phys.* **2008**, *4*, 627−630.
(22) Zhang, Y.; Tang, T. T.; Girit, C.; Hao, Z.; Martin, M. C.; Zettl, A.; Crommie, M. F.; Shen, Y. R.; Wang, F. *Nature* **2009**, *459*, 820−823.
(23) Khodkov, T.; Khrapach, I.; Craciun, M. F.; Russo, S. *Nano Lett.* **2015**, *15*, 4429−4433.
(24) Lu, C. P.; Li, G.; Mao, J.; Wang, L. M.; Andrei, E. Y. *Nano Lett.* **2014**, *14*, 4628−4633.
(25) Chu, T.; Ilatikhameneh, H.; Klimeck, G.; Rahman, R.; Chen, Z. *Nano Lett.* **2015**, *15*, 8000−8007.
(26) Xue, J.; Sanchez-Yamagishi, J.; Bulmash, D.; Jacquod, P.; Deshpande, A.; Watanabe, K.; Taniguchi, T.; Jarillo-Herrero, P.; LeRoy, B. J. *Nat. Mater.* **2011**, *10*, 282−285.
(27) Yankowitz, M.; Xue, J.; Cormode, D.; Sanchez-Yamagishi, J. D.; Watanabe, K.; Taniguchi, T.; Jarillo-Herrero, P.; Jacquod, P.; LeRoy, B. J. *Nat. Phys.* **2012**, *8*, 382−386.
(28) Lin, C.; Grassi, R.; Low, T.; Helmy, A. S. *Nano Lett.* **2016**, *16*, 1683−1689.
(29) Whitney, W. S.; Sherrott, M. C.; Jariwala, D.; Lin, W. H.; Bechtel, H. A.; Rossman, G. R.; Atwater, H. A. *Nano Lett.* **2017**, *17*, 78−84.
(30) Deng, B.; Tran, V.; Jiang, H.; Li, C.; Xie, Y.; Guo, Q.; Wang, X.; Tian, H.; Wang, H.; Cha, J. J.; Xia, Q. 2016, arXiv preprint arXiv:1612.04475.
(31) Yuan, S.; van Veen, E.; Katsnelson, M. I.; Roldán, R. *Phys. Rev. B: Condens. Matter Mater. Phys.* **2016**, *93*, 245433.
(32) Liu, Q.; Zhang, X.; Abdalla, L. B.; Fazzio, A.; Zunger, A. *Nano Lett.* **2015**, *15*, 1222−1228.
(33) Wood, J. D.; Wells, S. A.; Jariwala, D.; Chen, K. S.; Cho, E.; Sangwan, V. K.; Liu, X.; Lauhon, L. J.; Marks, T. J.; Hersam, M. C. *Nano Lett.* **2014**, *14*, 6964−6970.
(34) Castellanos-Gomez, A.; Vicarelli, L.; Prada, E.; Island, J. O.; Narasimha-Archarya, K. L.; Blanter, S. I.; Groenendijk, D. J.; Buscema,

DOI: 10.1021/acs.nanolett.6b05381
Nano Lett. 2017, 17, 1970−1977

M.; Steele, G. A.; Alvarez, J. V.; Zandbergen, H. W.; Palacios, J. J.; van der Zant, H. S. J. *2D Mater.* **2014**, *1*, 025001.
(35) Favron, A.; Gaufrès, E.; Fossard, F.; Phaneuf-L'Heureux, A. L.; Tang, N. Y.; Lévesque, P. L.; Loiseau, A.; Leonelli, R.; Francoeur, S.; Martel, R. *Nat. Mater.* **2015**, *14*, 826−832.
(36) Kim, J.-S.; Liu, Y.; Zhu, W.; Kim, S.; Wu, D.; Tao, L.; Dodabalapur, A.; Lai, K.; Akinwande, D. *Sci. Rep.* **2015**, *5*, 8989.
(37) Castellanos-Gomez, A.; Buscema, M.; Molenaar, R.; Singh, V.; Janssen, L.; van der Zant, H. S.; Steele, G. A. *2D Mater.* **2014**, *1*, 011002.
(38) Aierken, Y.; Çakır, D.; Sevik, C.; Peeters, F. M. *Phys. Rev. B: Condens. Matter Mater. Phys.* **2015**, *92*, 081408.
(39) Liang, L.; Wang, J.; Lin, W.; Sumpter, B. G.; Meunier, V.; Pan, M. *Nano Lett.* **2014**, *14*, 6400−6406.
(40) Zhang, C. D.; Lian, J. C.; Yi, W.; Jiang, Y. H.; Liu, L. W.; Hu, H.; Xiao, W. D.; Du, S. X.; Sun, L. L.; Gao, H. J. *J. Phys. Chem. C* **2009**, *113*, 18823−18826.
(41) Ugeda, M. M.; Bradley, A. J.; Shi, S. F.; Felipe, H.; Zhang, Y.; Qiu, D. Y.; Ruan, W.; Mo, S. K.; Hussain, Z.; Shen, Z. X.; Wang, F. *Nat. Mater.* **2014**, *13*, 1091−1095.
(42) Miller, D. A. B.; Chemla, D. S.; Schmitt-Rink, S. *Phys. Rev. B: Condens. Matter Mater. Phys.* **1986**, *33*, 6976.
(43) Klein, J.; Wierzbowski, J.; Regler, A.; Becker, J.; Heimbach, F.; Müller, K.; Kaniber, M.; Finley, J. J. *Nano Lett.* **2016**, *16*, 1554−1559.
(44) Brar, V. W.; Decker, R.; Solowan, H. M.; Wang, Y.; Maserati, L.; Chan, K. T.; Lee, H.; Girit, Ç.O.; Zettl, A.; Louie, S. G.; Cohen, M. L. *Nat. Phys.* **2011**, *7*, 43−47.
(45) Luryi, S. *Appl. Phys. Lett.* **1988**, *52*, 501−503.
(46) Bostwick, A.; Ohta, T.; Seyller, T.; Horn, K.; Rotenberg, E. *Nat. Phys.* **2007**, *3*, 36−40.
(47) Brar, V. W.; Wickenburg, S.; Panlasigui, M.; Park, C. H.; Wehling, T. O.; Zhang, Y.; Decker, R.; Girit, Ç.; Balatsky, A. V.; Louie, S. G.; Zettl, A. *Phys. Rev. Lett.* **2010**, *104*, 036805.
(48) Girard, J. C.; Lemaître, A.; Miard, A.; David, C.; Wang, Z. Z. *J. Vac. Sci. Technol. B* **2009**, *27*, 891−894.
(49) Zhang, G.; Chaves, A.; Huang, S.; Song, C.; Low, T.; Yan, H. 2016, *arXiv preprint arXiv:1607.08049*.
(50) Sirtori, C.; Faist, J.; Capasso, F.; Cho, A. Y. *Pure Appl. Opt.* **1998**, *7*, 373.
(51) Rogalski, A. *Infrared Phys. Technol.* **2007**, *50*, 240−252.
(52) Sun, Z.; Martinez, A.; Wang, F. *Nat. Photonics* **2016**, *10*, 227−238.

DOI: 10.1021/acs.nanolett.6b05381
Nano Lett. 2017, 17, 1970−1977